Hindawi
Wireless Communications and Mobile Computing
Volume 2022, Article ID 8227307, 14 pages
https://doi.org/10.1155/2022/8227307

Research Article

Intelligent Teaching of Tennis Based on Human Skeleton Node Model

Daibin Peng[1] **and Yonghong Liu**[2]

[1]*Wuhan City Polytechnic, Hubei 430064, China*
[2]*Hubei University, Wuhan 430062, China*

Correspondence should be addressed to Yonghong Liu; 20040752@hubu.edu.cn

Received 10 March 2022; Revised 8 April 2022; Accepted 15 April 2022; Published 23 May 2022

Academic Editor: Mu En Wu

In order to improve the effect of tennis intelligent teaching, this paper combines the human skeleton node model to construct a tennis intelligent teaching model. Aiming at the fact that there are errors in model identification and positional disturbances such as friction which cannot be avoided in actual tennis teaching, an effective sliding mode control strategy based on disturbance observer is presented. Moreover, this paper builds a simulation model through MATLAB/Simulink to verify the influence of the three parameters of inertia, damping, and stiffness in the admittance model on the control performance. Then, this paper combines the admittance control theory to analyze the difference between the active mode and the passive mode and the main functions of the two control modes and constructs an intelligent simulation system. The experimental study shows that the tennis intelligent teaching model based on the human skeleton node model has good effects in tennis action correction and tennis-teaching effect improvement.

1. Introduction

The current tennis classroom teaching focuses on application, understanding, and memory. The future classroom teaching should be innovative, challenging, and advanced. The athletic ability and sports foundation of the students in the tennis option course are uneven. Most boys have stronger athletic ability while girls are slightly weaker. Therefore, it is recommended that teachers carry out more personalized and innovative teaching methods and grasp the differentiated characteristics of students' athletic ability to carry out teaching in accordance with their aptitude. Teachers can use hierarchical teaching methods, heuristic teaching methods, problem-oriented teaching methods, etc. to improve the bilateral roles of teachers and students in traditional tennis teaching. At the same time, teachers can establish a student-centered teaching method, which fully reflects the main body status of students and cultivates students' thinking ability. At the same time, teachers can use the convenient functions of modern educational information technology to carry out mixed tennis teaching, by combining various teaching platforms or teaching software. By allowing students to watch tennis technology videos online, more intuitive teaching can be achieved, so that students can more thoroughly understand the principles of action learning and more firmly grasp the learned knowledge.

Active learning and passive learning of tennis techniques have very different learning outcomes. Passive learning mainly imitates the basic skills of tennis through the teacher's explanation and demonstration and cannot make the students understand the principle of action technology very clearly. Active learning is mainly through the method of self-learning and then taught by teachers in the process of self-learning before and after class. In this learning process, students can more thoroughly understand the principles of tennis action techniques, and it is easier to grasp the key points and difficulties of teaching. There is also greater clarity on the fallibility of tennis action technique. Therefore, it is necessary to transform students learning through traditional teaching; to a certain extent, it can cultivate students' life-long sports-learning ability and lay a foundation for students' life-long sports activities. At present,

more than 1/3 of colleges and universities in my country have set up tennis elective courses. More than a quarter of colleges and universities offer tennis sports options. Tennis has played an active role in promoting college students' physical health, developing lifelong physical exercise habits, and cultivating sportsmanship. However, in the practice of tennis teaching and research in colleges and universities, it is found that the vast majority of students think that tennis is difficult and cannot persist for a long time after learning. The fundamental reason is that, on the one hand, compared with small ball sports such as table tennis and badminton, tennis has the characteristics of being difficult to get started and slow to learn. With regard to the teaching method, the practice content is single, the practice method is boring, and the organization method is dominated by teachers, which do not mobilize the autonomy and enthusiasm of the students and do not give full play to the creativity and initiative of the students. Therefore, in order to further promote the teaching of tennis sports optional courses in colleges and universities, help college students to master tennis skills, and lay a good foundation for better development of tennis in the future, this paper studies the tennis-teaching methods in colleges and universities and provides a useful reference for the teaching of tennis teachers in colleges and universities.

Based on the above analysis, intelligent tennis teaching can solve most of the problems existing in the current methods of tennis teaching. Therefore, this paper combines the human skeleton node model to construct a tennis intelligent teaching model to improve the effect of tennis intelligent teaching and further improve the quality of tennis teaching.

2. Related Work

Accurate skeleton information can also be used as important spatial literature information for bone skinning in the subsequent process of automatic character modeling, improving the accuracy of deformation drive establishment between bones and model skin. At the same time, skeletons that conform to the laws of human kinematics are also in the process of motion data loading. The basic requirements of the model can make the model fit well the motion data obtained by motion extraction and retain to the greatest extent the characteristics of the original motion collected. Therefore, how to extract accurate skeleton data from the three-dimensional human body model and meet the requirements of motion data attachment is an important part of completing automatic character modeling [1].

The curve bones of a model often have hundreds of nodes, so the whole looks like a curve. However, to apply bones to motion rigs, you do not need so many points. Therefore, it is one of the keys to extract joint bones from curvilinear bones by downsampling the curvilinear bones and extracting a smaller number of joint point sets suitable for bone binding and motion data loading [2]. Downsampling is a multirate digital signal processing technique or the process of reducing the sampling rate of a signal, usually used to reduce the data transmission rate or data size. In the processing of curvilinear bones, the definition of downsampling is extended to process curvilinear bones, while reducing the number of nodes of curvilinear bones, while ensuring that key information is not lost [3]. The downsampling of curved bones mainly extracts the points containing important features in the bones. Among them, the connection point and the end point are the important point sets that can reflect the characteristics of the model. For all points in the model curve skeleton, they are classified according to how many nodes the node has a connection relationship with. The number 1 is the end point, the number 2 is the ordinary point, and the number more than 3 is the connection point. Taking the human body as an example, the joint points of the end of the hand, the end of the foot, and the head are the end points, and the neck joint and the hip joint are the connection points [4].

Software such as Kinect and Maya have their own standards, and in the face of different model types, the standard changes may also be quite large. After completing the curve skeleton extraction, the specific requirements of the key skeleton nodes that are sampled and retained are different in different application scenarios and model types [5]. In the literature [6], the method of topology refinement is used to gradually converge the surface of the model mesh; shrinking to the limit, the surface is concentrated near the expected skeleton node, and the center point in the tangential field is sampled and connected to obtain the model skeleton. This method has strong applicability and can obtain skeletons for any type of model, but the number of nodes and topology in the obtained skeleton will be affected by the shrinking process of the surface structure of the model, and the number and topology of nodes are random and redundant nodes are too many. In [7], a method is proposed to use the geodesic distance as a processing function to construct the Reeb graph of the model. This method does not complete the downsampling extraction of the joint points of the model but only completes the segmentation of the model and obtains rough end points. It is used as the limb node of the character model, and it lacks the supplementary nodes required for the flexible movement of the three-dimensional character. In the literature [8], the curved bones extracted by the method based on distance transformation are affected by the changes of the surface of the model. When the surface features of the model are more complex, the connectivity of the curves is poor, so the connectivity of the obtained skeleton will also be poor. Only after calculating to connect the obtained skeleton can the key skeleton nodes be obtained by sampling. Literature [9] uses the Voronoi diagram to obtain the result of the model axis, which needs to be pruned; the complexity of the algorithm is relatively high; and it is difficult to downsample to a simple linear skeleton structure.

At present, the research methods of human gesture recognition mainly include statistical-based algorithms [10] and grammar-based algorithms (Finite State Machine (FSM), Context-Free Text (CFG)) [11]. Among the algorithms for human pose research, template matching has better recognition accuracy and robustness than other algorithms, but the establishment of the model requires a

large amount of data and the calculation of features is complex [12]. Literature [13] proposed a static 3D gesture recognition based on Kinect skeleton data. By obtaining the hand angle feature vector to determine the posture template to be measured, the posture to be measured and the posture template are optimally matched. Due to the persistence of the behavior time interval and the image and due to the influence of noise, each frame of image cannot be detected and recognized in real time. Literature [14] proposed a real-time multiperson human pose recognition based on the similarity of parts. The algorithm adopts a bottom-up approach. First, the key points of the human body are detected, and then, a vector field is established to infer the key parts and connect them. Finally, the deep-learning network structure is used to construct a feature image set for attitude prediction; however, this algorithm has certain limitations, only considering the position information of the key points of the limbs and ignoring the invariance of rotation and scale, so the attitude can only be performed in the local area to predict connections. Literature [15] proposes a Kinect gesture control robot based on the convolutional neural network and FastDTW, which extracts and processes the joint information of each frame of the captured image from the Kinect, establishes the derived images of all frames of gesture actions, and uses joint training and personal training performed with convolutional neural network (CNN) training, and finally, the mobile robot system is added to the trained system to control the movement of the robot according to the classification results of the pose algorithm. Literature [16] proposed the recognition of moving human behavior based on video stream, using the interframe difference method and the improved CV model algorithm to segment the moving human body, detecting the contour curve of the moving object, classifying the segmented contour with weighted motion string, and constructing the action string. Different weights are given to different poses at different times, and finally, the abnormal behavior of global motion information and local feature information is identified.

3. Human Skeleton Point Intelligent Model

We consider a second-order system as follows:

$$\begin{cases} \dot{x}_1 = x_2, \\ \dot{x}_2 = h(x) + g(x)u. \end{cases} \tag{1}$$

Among them, $\forall x, g(x) \geq g(0) > 0, g(x), h(x)$ are unknown nonlinear functions. The sliding mode control is used to design a control rate so that the system represented by (1) moves on the surface $s = a_1x_1 + x_2 = 0$. The choice of a_1 can control the convergence speed of the system as $x(t)$ tends to 0 when time tends to infinity.

The main design problem is how to switch the trajectory to the curve $s = a_1x_1 + x_2 = 0$ and keep it. Differentiating the curve, we can get

$$\dot{s} = a_1\dot{x}_1 + \dot{x}_2 = a_1x_2 + h(x) + g(x)u. \tag{2}$$

If there is some known function $\xi(x)$ such that the following inequality holds

$$\left|\frac{a_1x_2 + h(x)}{g(x)}\right| \leq \xi(x), \quad \forall x \in R^2. \tag{3}$$

We choose the Lyapunov function $V = (1/2)s^2$ and derive it to get

$$\dot{V} = s\dot{s} = s[a_1x_2 + h(x)] + g(x)su \leq g(x)|s|\xi(x) + g(x)su. \tag{4}$$

We take

$$u = -\beta(x)\ \text{sgn}\ (s). \tag{5}$$

Among them, $\beta(x) \geq \xi(x) + \beta_0, \beta_0 > 0$. Then, there is

$$\dot{V} \leq g(s)|s|\xi(x) - g(x)[\xi(x) + \beta_0]s\ \text{sgn}\ (s) = -g(x)\beta_0|s| \leq -g_0\beta_0|s|. \tag{6}$$

Therefore, the motion trajectory of the controlled object can reach the curve $s = 0$ in a limited time. Moreover, it can be seen from (6) that the motion trajectory will not leave once it reaches the curve. A typical phase diagram under the sliding mode control is shown in Figure 1.

In the actual process, it is difficult to realize the high-performance position tracking control of the robot due to the existence of external disturbances. The disturbance observer is an effective solution, and the disturbance observer based on the following model is discussed.

$$H(\theta)\ddot{\theta} + C\left(\theta, \dot{\theta}\right)\dot{\theta} + G(\theta) = T. \tag{7}$$

The unknown external disturbance existing in the two-degree-of-freedom lower-limb exoskeleton system can be collectively expressed as $d \in R$. Then, after considering the disturbance, formula (7) can be expressed as

$$H(\theta)\ddot{\theta} + C\left(\theta, \dot{\theta}\right)\dot{\theta} + G(\theta) = T + d. \tag{8}$$

That is,

$$d = H(\theta)\ddot{\theta} + C\left(\theta, \dot{\theta}\right)\dot{\theta} + G(\theta) - T. \tag{9}$$

The basic idea of the disturbance observer is to compare the difference between the actual output and the estimated output of the system and use this difference to make real-time corrections to the system estimate.

$$\begin{aligned} \dot{\widehat{d}} = L\left(\theta, \dot{\theta}\right)\left(d - \widehat{d}\right) = -L\left(\theta, \dot{\theta}\right)\widehat{d} + L\left(\theta, \dot{\theta}\right)d = -L\left(\theta, \dot{\theta}\right)\widehat{d} \\ + L\left(\theta, \dot{\theta}\right)\left[H(\theta)\ddot{\theta} + C\left(\theta, \dot{\theta}\right)\dot{\theta} + G(\theta) - T\right]. \end{aligned} \tag{10}$$

Among them, $\widehat{d}$ represents the observation of the

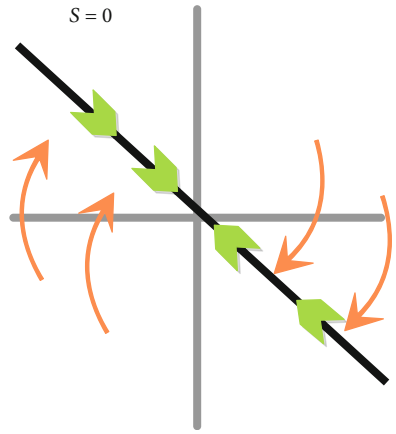

Figure 1: Typical phase diagram under sliding mode control.

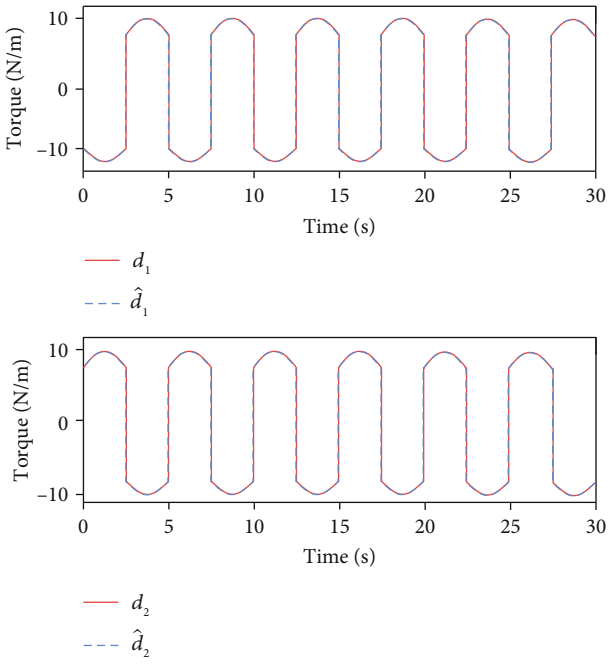

Figure 2: Observation results of the disturbance observer.

disturbance. In the actual process, it is generally impossible to know the prior information of the differential of the interference term, but the change of the interference is often slow, and it can be assumed that the differential term is 0, that is,

$$\dot{d} = 0. \tag{11}$$

The observation error is

$$e(t) = d - \hat{d}. \tag{12}$$

That is,

$$\dot{e}(t) = \dot{d} - \dot{\hat{d}} = -L\left(\theta, \dot{\theta}\right)\left(d - \hat{d}\right) = -L\left(\theta, \dot{\theta}\right)e. \tag{13}$$

In the actual process, since it is difficult to obtain an accurate acceleration signal by differentiating the speed signal of the robot, the observer shown in (10) cannot achieve the predetermined effect in practical engineering. It is necessary to design a more practical nonlinear disturbance observer.

The auxiliary vector is

$$z = \hat{d} - p\left(\theta, \dot{\theta}\right). \tag{14}$$

Among them, $z \in R^2$, and the nonlinear vector $p(\theta, \dot{\theta})$ is the function vector to be designed. Differentiating the above equation, we can get

$$\dot{z} = \dot{\hat{d}} - \frac{dp\left(\theta, \dot{\theta}\right)}{dt}. \tag{15}$$

$L(\theta, \dot{\theta})$ in formula (10) is given by

$$L\left(\theta, \dot{\theta}\right)H(\theta)\ddot{\theta} = \frac{dp\left(\theta, \dot{\theta}\right)}{dt} = \left[\frac{dp\left(\theta, \dot{\theta}\right)}{d\theta}\ \frac{dp\left(\theta, \dot{\theta}\right)}{d\dot{\theta}}\right]\begin{bmatrix}\dot{\theta}\\ \ddot{\theta}\end{bmatrix}. \tag{16}$$

We obtain

$$\dot{z} = \dot{\hat{d}} - \frac{dp\left(\theta, \dot{\theta}\right)}{dt} = \dot{\hat{d}} - L\left(\theta, \dot{\theta}\right)H(\theta)\ddot{\theta}. \tag{17}$$

Bringing (10) into (17), we get

$$\begin{aligned}\dot{z} = \dot{\hat{d}} - L\left(\theta, \dot{\theta}\right)H(\theta)\ddot{\theta} &= -L\left(\theta, \dot{\theta}\right)\hat{d} + L\left(\theta, \dot{\theta}\right)\left[H(\theta)\ddot{\theta}\right.\\ &\left. + C\left(\theta, \dot{\theta}\right)\dot{\theta} + G(\theta) - T\right] - L\left(\theta, \dot{\theta}\right)H(\theta)\ddot{\theta} = -L\left(\theta, \dot{\theta}\right)\hat{d}\\ &+ L\left(\theta, \dot{\theta}\right)\left[C\left(\theta, \dot{\theta}\right)\dot{\theta} + G(\theta) - T\right].\end{aligned} \tag{18}$$

Bringing (14) into (18), we get

$$\begin{aligned}\dot{z} &= -L\left(\theta, \dot{\theta}\right)\left[z + p\left(\theta, \dot{\theta}\right)\right] + L\left(\theta, \dot{\theta}\right)\left[C\left(\theta, \dot{\theta}\right)\dot{\theta} + G(\theta) - T\right]\\ &= -L\left(\theta, \dot{\theta}\right)z + L\left(\theta, \dot{\theta}\right)\left[C\left(\theta, \dot{\theta}\right)\dot{\theta} + G(\theta) - T - p\left(\theta, \dot{\theta}\right)\right].\end{aligned} \tag{19}$$

To sum up, the nonlinear disturbance observer that does not need the acceleration information of the disturbance signal can be designed in the following form:

$$\begin{cases}\dot{z} = -L\left(\theta, \dot{\theta}\right)z + L\left(\theta, \dot{\theta}\right)\left[C\left(\theta, \dot{\theta}\right)\dot{\theta} + G(\theta) - T - p\left(\theta, \dot{\theta}\right)\right],\\ \hat{d} = z + p\left(\theta, \dot{\theta}\right).\end{cases} \tag{20}$$

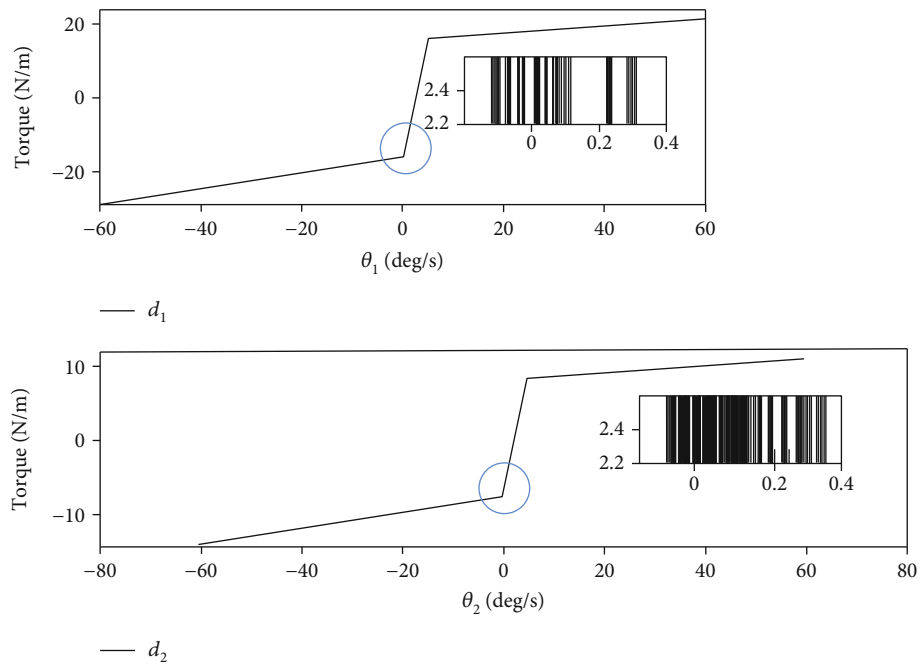

Figure 3: Relationship between friction disturbance and joint speed.

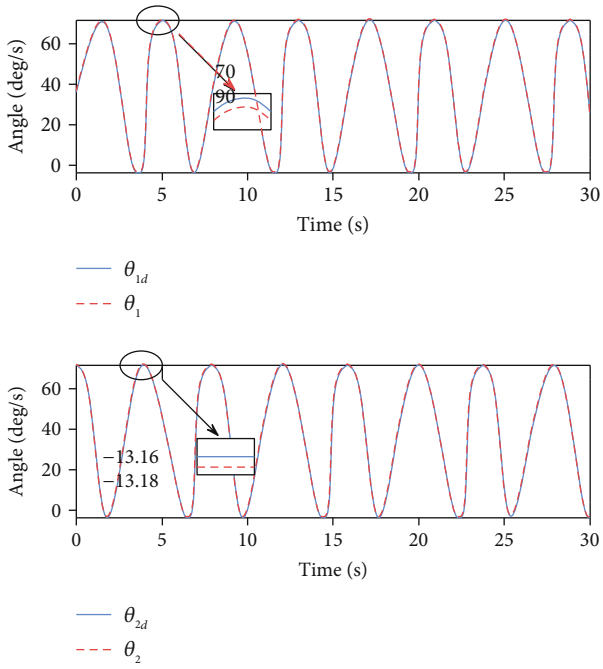

Figure 4: Angle tracking of hip and knee joints.

Bringing (15), (16), and (20) into (13), we get

$$\begin{aligned}\dot{e} = \dot{d} - \dot{\hat{d}} = -\dot{\hat{d}} = -\dot{z} - \frac{dp(\theta,\theta)}{dt} = L\left(\theta,\dot{\theta}\right)z \\ - L\left(\theta,\dot{\theta}\right)\left[C\left(\theta,\dot{\theta}\right)\dot{\theta} + G(\theta) - T - p\left(\theta,\dot{\theta}\right)\right] \\ - L\left(\theta,\dot{\theta}\right)H(\theta)\ddot{\theta} = L\left(\theta,\dot{\theta}\right)\left[z + p\left(\theta,\dot{\theta}\right)\right] \\ - L\left(\theta,\dot{\theta}\right)\left[H(\theta)\ddot{\theta} + C\left(\theta,\dot{\theta}\right)\dot{\theta} + G(\theta) - T\right].\end{aligned} \tag{21}$$

Therefore, we get

$$\dot{e} = L\left(\theta,\dot{\theta}\right)\hat{d} - L\left(\theta,\dot{\theta}\right)d = -L\left(\theta,\dot{\theta}\right)\left(d - \hat{d}\right) = -L\left(\theta,\dot{\theta}\right)e. \tag{22}$$

That is,

$$\dot{e} + L\left(\theta,\dot{\theta}\right)e = 0. \tag{23}$$

Therefore, the observation error can be exponentially approached to 0 by designing the function $L(\theta,\dot{\theta})$.

For the following two-degree-of-freedom lower-limb exoskeleton Lagrange dynamic model,

$$H(\theta)\ddot{\theta} + C\left(\theta,\dot{\theta}\right)\dot{\theta} + G(\theta) = T + d. \tag{24}$$

Among them, H, C, and G represent the inertia matrix, Coriolis matrix, and gravity matrix, respectively, and their values can be obtained by the model identification method described in Section 3. T is the control torque, and d is the unknown disturbance.

θ_d is the expected command signal of the exoskeleton joint, $e = \theta_d - \theta$ is the error signal, and the designed sliding surface is

$$s = \dot{e} + \mathrm{K}e. \tag{25}$$

Among them, $K = \mathrm{diag}\,(k_1, k_2, \cdots k_n), k_i > 0$. The

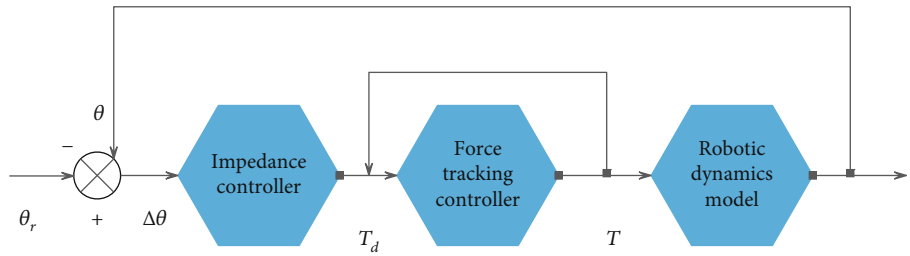

Figure 5: Block diagram of impedance control.

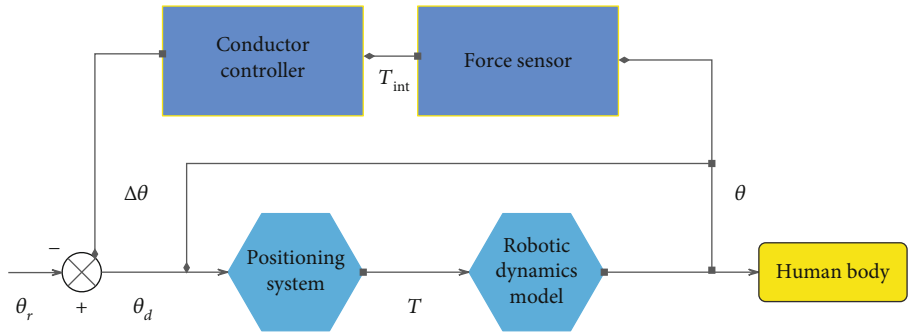

Figure 6: Block diagram of admittance control principle.

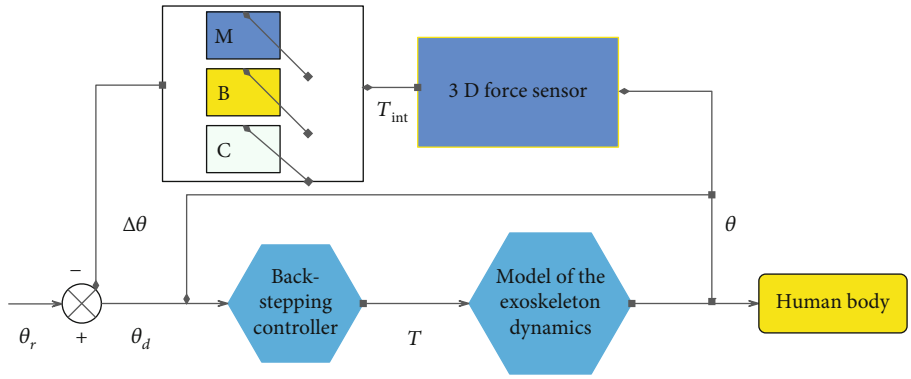

Figure 7: Control block diagram of admittance parameter simulation.

following Lyapunov functions are chosen:

$$V = \frac{1}{2}s^T Hs. \tag{26}$$

Derivating the above formula, we can get

$$\dot{V} = \frac{1}{2}s^T \dot{H}s + s^T H\dot{s} = \frac{1}{2}s^T (\dot{H} - 2C)s + s^T Cs + s^T H\dot{s} = s^T (Cs + H\dot{s}). \tag{27}$$

Differentiating (25) and bringing it into (27), we get

$$\begin{aligned} \dot{V} &= s^T[Cs + H(\ddot{e} + K\dot{e})] = s^T\left[Cs + H\left(\ddot{\theta}_d - \ddot{\theta}\right) + HK\dot{e}\right] \\ &= s^T\left[C\dot{e} + CKe + H\ddot{\theta}_d + C\dot{\theta} + G - T - d + HK\dot{e}\right] \\ &= s^T\left[C\dot{e} + CKe + H\left(\ddot{\theta}_d + K\dot{e}\right) + C\dot{\theta} + G - T - d\right] \\ &= s^T\left[C\left(\dot{\theta}_d + Ke\right) + H\left(\ddot{\theta}_d + K\dot{e}\right) + G - T - d\right]. \end{aligned} \tag{28}$$

The control rate is

$$T = \bar{H}\left(\ddot{\theta}_d + K\dot{e}\right) + \bar{C}\left(\dot{\theta}_d + Ke\right) + \bar{G} - \hat{d} + \Gamma\,\mathrm{sgn}\,(s). \tag{29}$$

Among them, $\bar{H}$, $\bar{C}$, $\bar{G}$ represent the nominal value of H, C, and G, respectively, which can be regarded as the identified data in practical engineering. H, C, and G represent the actual physical parameters of the controlled object, and there will be a certain error between the nominal value and the actual value, which is taken as $\Delta H = H - \bar{H}$, $\Delta C = C - \bar{C}$, $\Delta G = G - \bar{G}$. $\hat{d}$ represents the nominal value of unmodeled disturbances such as friction, which is taken as $\Delta d = d - \hat{d}$ and which is generally not available in practice and can be resolved by disturbance observers, which will be discussed below.

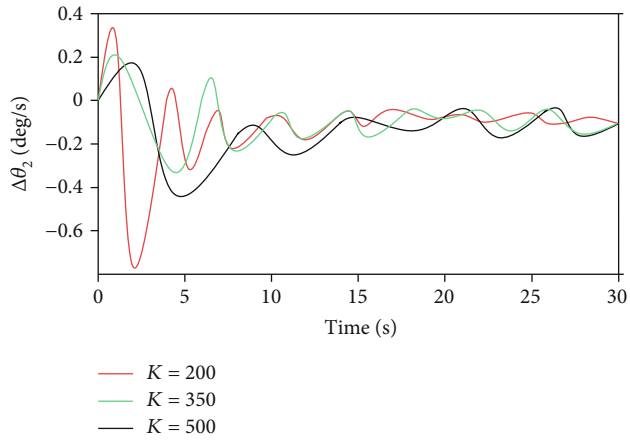

Figure 8: Influence of knee stiffness coefficient on reference trajectory.

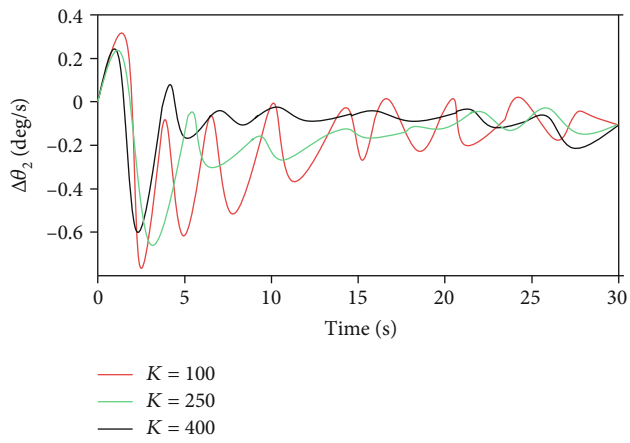

Figure 9: Influence of knee joint damping coefficient on reference trajectory.

Bringing (29) into (28), we get

$$\dot{V} = s^T\left[\Delta C\left(\dot{\theta}_d + Ke\right) + \Delta H\left(\ddot{\theta}_d + K\dot{e}\right) + G - \Delta d\right] - \Gamma|s|. \tag{30}$$

Among them, $\Gamma = \text{diag}\,(\gamma_1, \gamma_2, \cdots \gamma_n)(\gamma_i > 0)$, and if we take

$$\gamma_i > |\Delta C|_{\max}\left|\dot{\theta}_d + Ke\right| + |\Delta H|_{\max}\left|\ddot{\theta}_d + K\dot{e}\right| + |\Delta d|_{\max} + |\Delta G|_{\max}. \tag{31}$$

Then, (31) can be guaranteed to be less than or equal to 0.

The following is a nonlinear disturbance observer for the two-degree-of-freedom lower-extremity exoskeleton described in (24) to estimate the unmodeled disturbance d. The inertia matrix of the two-degree-of-freedom lower-extremity exoskeleton can be written in the following form:

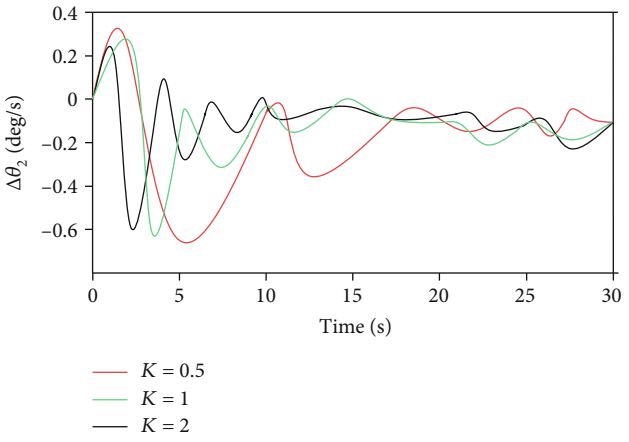

Figure 10: Influence of knee joint inertia coefficient on reference trajectory.

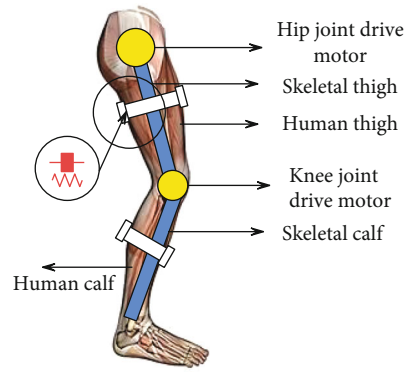

Figure 11: Simplified schematic diagram of human-machine coupling.

$$H = \begin{bmatrix} \Phi^{(1)} + 2\Phi^{(3)}\cos(\theta_2) & \Phi^{(2)} + \Phi^{(3)}\cos(\theta_2) \\ \Phi^{(2)} + \Phi^{(3)}\cos(\theta_2) & \Phi^{(2)} \end{bmatrix}. \tag{32}$$

Among them, $\Phi^{(1)}, \Phi^{(2)}, \Phi^{(3)}, \Phi^{(4)}$ is the inertial parameter of the exoskeleton, which is related to the physical parameters of the mechanical mechanism, motor, and load. When the function $p(\theta, \dot{\theta})$ in the observer (20) is taken as

$$p\left(\theta, \dot{\theta}\right) = c\begin{bmatrix} \dot{\theta}_1 \\ \dot{\theta}_1 + \dot{\theta}_2 \end{bmatrix}. \tag{33}$$

Among them, c is the maximum velocity of the knee joint, at which time the observer (20) is globally asymptotically stable. The detailed derivation process is given below.

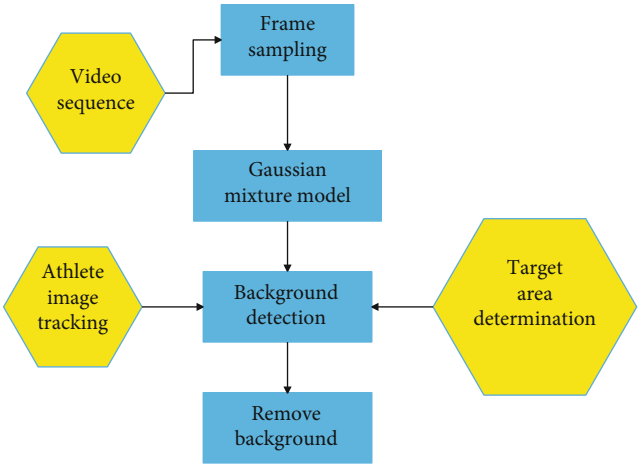

(a) The athlete-centered background color removal

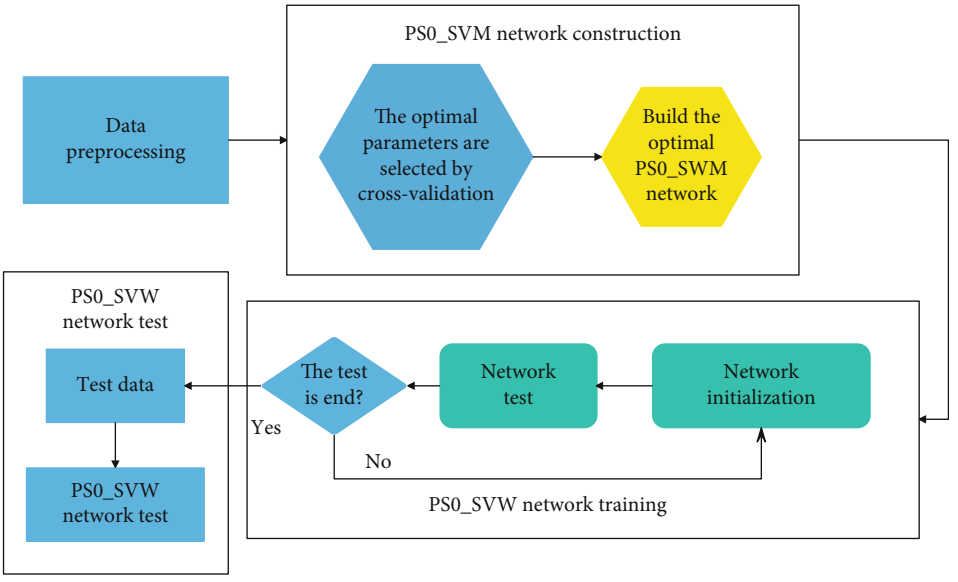

(b) The overall process of the PSO-SVM model

Figure 12: The intelligent teaching process of tennis based on the human skeleton node model.

According to formula (33), it can be known that

$$\frac{dp\left(\theta,\dot{\theta}\right)}{dt}=c\begin{bmatrix}\ddot{\theta}_1\\ \ddot{\theta}_1+\ddot{\theta}_2\end{bmatrix}=c\begin{bmatrix}1&0\\1&1\end{bmatrix}\ddot{\theta}. \tag{34}$$

From formula (16), we can get

$$L\left(\theta,\dot{\theta}\right)H(\theta)\ddot{\theta}=\frac{dp\left(\theta,\dot{\theta}\right)}{dt}=c\begin{bmatrix}1&0\\1&1\end{bmatrix}\ddot{\theta}. \tag{35}$$

According to the structural characteristics of the exoskeleton, it can be known that the inertia matrix H is positive definite and invertible. Therefore, by (35), we get

$$L\left(\theta,\dot{\theta}\right)=\frac{dp\left(\theta,\dot{\theta}\right)}{dt}=c\begin{bmatrix}1&0\\1&1\end{bmatrix}H^{-1}(\theta). \tag{36}$$

According to the theory of matrix decomposition, we can get

$$H=\begin{bmatrix}1&1\\0&1\end{bmatrix}\begin{bmatrix}\Phi^{(1)}-\Phi^{(2)}&\Phi^{(3)}\cos\left(\theta_2\right)\\ \Phi^{(3)}\cos\left(\theta_2\right)&\Phi^{(2)}\end{bmatrix}\begin{bmatrix}1&0\\1&1\end{bmatrix}. \tag{37}$$

Among them,

$$\begin{bmatrix}\Phi^{(1)}-\Phi^{(2)}&\Phi^{(3)}\cos\left(\theta_2\right)\\ \Phi^{(3)}\cos\left(\theta_2\right)&\Phi^{(2)}\end{bmatrix}=\bar{H}. \tag{38}$$

Table 1: The tennis action correction effect of the tennis intelligent teaching model based on the human skeleton node model.

Number	Action correction
1	79.14
2	71.23
3	79.07
4	81.52
5	69.34
6	80.32
7	75.15
8	80.77
9	81.59
10	82.60
11	69.98
12	74.66
13	80.17
14	78.22
15	69.27
16	77.79
17	71.11
18	80.38
19	82.04
20	83.05
21	70.14
22	71.51
23	81.94
24	72.59
25	81.82
26	78.34
27	70.73
28	83.54
29	69.40
30	75.63
31	72.81
32	74.17
33	78.22
34	73.06
35	76.79
36	73.29
37	79.07
38	73.42
39	70.56
40	72.29
41	78.29
42	70.15
43	74.95
44	79.51
45	83.26
46	73.65
47	77.78
48	82.37
49	83.92
50	72.54
51	72.08
52	69.83
53	75.87
54	76.45
55	80.92
56	73.26
57	77.11
58	78.33
59	76.42
60	79.14

Then, we can get

$$H^{-1} = \begin{bmatrix} 1 & 0 \\ -1 & 1 \end{bmatrix} \bar{H}^{-1} \begin{bmatrix} 1 & -1 \\ 0 & 1 \end{bmatrix}. \tag{39}$$

Therefore, (36) can be written as

$$L\left(\theta, \dot{\theta}\right) = \frac{dp\left(\theta, \dot{\theta}\right)}{dt} = c\bar{H}^{-1}(\theta) \begin{bmatrix} 1 & -1 \\ 0 & 1 \end{bmatrix}. \tag{40}$$

The Lyapunov function is

$$V(e, \theta) = e^T \bar{H}(\theta) e. \tag{41}$$

Differentiating the above formula, we get

$$\frac{dV(e,\theta)}{dt} = \frac{\partial V(e,\theta)}{\partial e}\dot{e} + \frac{\partial V(e,\theta)}{\partial \theta}\dot{\theta} = 2e^T \bar{H}(\theta)\dot{e} + e^T \bar{H}\left(\dot{\theta}\right)e. \tag{42}$$

Through combining (23), we can get

$$\frac{dV(e,\theta)}{dt} = -2e^T \bar{H}(\theta) L\left(\theta, \dot{\theta}\right) e + e^T \bar{H}\left(\dot{\theta}\right) e. \tag{43}$$

According to the definition of $\bar{H}$, we can get

$$\bar{H}\left(\dot{\theta}\right) = \begin{bmatrix} 0 & -\Phi^{(3)} \sin\left(\theta_2\right) \cdot \dot{\theta}_2 \\ -\Phi^{(3)} \sin\left(\theta_2\right) \cdot \dot{\theta}_2 & 0 \end{bmatrix}. \tag{44}$$

Table 2: Tennis-teaching effect of tennis intelligent teaching model based on human skeleton node model.

Number	Tennis teaching
1	83.02
2	75.05
3	82.90
4	77.92
5	85.26
6	86.16
7	79.51
8	77.09
9	80.30
10	80.57
11	79.68
12	77.92
13	84.74
14	76.65
15	87.98
16	85.57
17	75.64
18	83.90
19	75.98
20	82.97
21	77.91
22	74.88
23	76.26
24	87.95
25	87.87
26	74.60
27	74.47
28	83.25
29	74.01
30	74.66
31	85.39
32	79.96
33	83.39
34	77.09
35	80.68
36	83.60
37	79.88
38	81.54
39	81.15
40	79.40
41	76.05
42	84.89
43	83.21
44	81.17
45	84.20
46	83.68
47	76.37
48	80.02
49	81.99
50	76.26
51	79.70
52	85.02
53	86.63
54	75.74
55	80.14
56	87.30
57	77.04
58	80.99
59	86.34
60	75.53

By combining (40), (43), and (44), we get

$$\begin{aligned}\frac{dV(e,\theta)}{dt} &= -2ce^T\begin{bmatrix}1 & -1\\ 0 & 1\end{bmatrix}e \\ &\quad + e^T\begin{bmatrix}0 & -\Phi^{(3)}\sin(\theta_2)\cdot\dot{\theta}_2\\ -\Phi^{(3)}\sin(\theta_2)\cdot\dot{\theta}_2 & 0\end{bmatrix}e \\ &= -e^T\begin{bmatrix}2c & -c+\Phi^{(3)}\sin(\theta_2)\cdot\dot{\theta}_2\\ -c+\Phi^{(3)}\sin(\theta_2)\cdot\dot{\theta}_2 & 2c\end{bmatrix}e.\end{aligned} \tag{45}$$

In order to ensure that the differential of the designed Lyapunov function is negative, it is necessary to ensure that the second term of the above formula is positive definite. From the judgment condition of the negative definite matrix, it can be known that the main subforms of each order of the matrix should be positive; that is, they should satisfy

$$\begin{cases}2c > 0,\\ \det\begin{bmatrix}2c & -c+\Phi^{(3)}\sin(\theta_2)\cdot\dot{\theta}_2\\ -c+\Phi^{(3)}\sin(\theta_2)\cdot\dot{\theta}_2 & 2c\end{bmatrix} > 0.\end{cases} \tag{46}$$

From the inequality equations of (46), we can get

$$c > \Phi^{(3)}\dot{\theta}_{2\,\max}. \tag{47}$$

Among them, $\dot{\theta}_{2\,\max}$ represents the maximum value of the knee joint velocity, which can guarantee (45) negative definiteness, and the designed disturbance observer is globally asymptotically stable.

Based on the above discussion, for the two-degree-of-freedom lower-extremity exoskeleton represented by (24), it can be driven by the control rate shown in equation (29). The unknown disturbance in the formula can be observed and estimated by the disturbance observers (20) and (33).

In order to verify the effect of the above-mentioned adaptive synovial controller, a simulation model was built using MATLAB/Simulink for numerical simulation verification. The two-degree-of-freedom lower-limb exoskeleton represented by (24) is driven using the control rate shown in formula (29). The unknown disturbance $\widehat{d}$ in formula (29) is estimated by the disturbance observers (20) and (33).

The specific parameters are set as follows. (24) can be expressed in the form of (28), where $\Phi^{(1)} = 25.68, \Phi^{(2)} = 6.91, \Phi^{(3)} = 1.32, \Phi^{(4)} = -11.68, a_{th} = 0.38m$, and

$$\bar{H} = 0.8 * H, \bar{C} = 0.8 * C, \bar{G} = 0.8 * G, K = \begin{bmatrix} 200 & 0 \\ 0 & 30 \end{bmatrix}. \tag{48}$$

Γ takes the value according to (31), and it can be seen from the calculation that c is 3000 in (33) to satisfy condition (47). For the convenience of simulation verification, the disturbance d is assumed to be the simplified friction model, namely,

$$d = \begin{bmatrix} z_1 \operatorname{sgn}\left(\dot{\theta}_1\right) + k_1\dot{\theta}_1 \\ z_2 \operatorname{sgn}\left(\dot{\theta}_2\right) + k_2\dot{\theta}_2 \end{bmatrix}, \tag{49}$$

where $z_1 = 13, z_2 = 10, k_1 = 3, k_2 = 2$. The expected trajectories of the hip and knee joints are taken as $\theta_{1d} = 0.565 + 0.655 \sin(0.5\pi t), \theta_{2d} = -0.925 + 0.695 \cos(0.5\pi t)$, respectively.

The simulation results are shown below. Figure 2 shows the observation effects of the disturbance observers (20) and (33). It can be clearly seen from the figure that the results of the observer are basically consistent with the actual interference, which proves the effectiveness of the proposed interference observer.

Figure 3 shows the corresponding relationship between joint friction and joint velocity, where the abscissa represents the angular velocity of the joint, and the ordinate represents the friction torque received by the joint. It can be seen from the figure that the frictional force on the hip joint is greater than that on the knee joint, and the direction of the frictional force changes back and forth near the speed zero of the two joints, which is in line with the actual law.

Figure 4 shows the angle following of the hip and knee joints of the 2DOF lower-limb exoskeleton driven by the disturbance observer-based sliding mode controller. It can be clearly seen from the figure that under the action of the given controller, the actual angle of the exoskeleton is basically the same as the expected angle, despite the difference between the nominal model and the actual model, as well as frictional disturbances. Among them, the error of the hip joint is within 1 degree, and the error of the knee joint is within 0.1 degree, which achieves a good follow-up effect.

Through numerical simulation experiments, the effectiveness of the proposed sliding mode control based on disturbance observer is effectively verified.

The concepts of impedance and admittance originate from circuit theory, where voltage is usually referred to as a potential variable and current is referred to as a flow variable. The ratio of the potential variable to the flow variable is defined as the impedance, and the ratio of the flow variable to the potential variable is defined as the admittance. Considering that the dynamics of a mechanical system can often be described by Newton's second law, viscosity law, and Hooke's law, Hogan defines the impedance model of a mechanical system as the following forms of mass, spring, and damping:

$$M\Delta\ddot{\theta}(t) + B\Delta\dot{\theta}(t) + K\Delta\theta(t) = T_{\text{int}}. \tag{50}$$

Among them, the first item on the left describes the relationship between acceleration and force, which is represented by the inertia matrix M. The second term describes the relationship between velocity and force, which is characterized by the damping matrix B, and the third term describes the relationship between the position and force, which is characterized by the stiffness matrix K. $\Delta\theta(t)$ represents the difference between the desired trajectory of the joint and the reference trajectory:

$$\Delta\theta(t) = \theta_d(t) - \theta_r(t). \tag{51}$$

The transfer function of the impedance model can be obtained by calculating the Laplace transform of formula (50) as

$$\frac{T_{\text{int}}(s)}{\Delta\theta(s)} = M(s)s^2 + B(s)s + K. \tag{52}$$

The natural frequency of the system is $w_n = \sqrt{K/M}$, and the damping ratio is $\xi = B/2\sqrt{MK}$.

By adjusting the impedance parameters M, B, and K, the robot can have different interaction performance with the environment. The impedance controller generally needs to be used in conjunction with the force tracker; that is, the torque tracking control of the joint needs to be realized before the impedance control can be used. Impedance control is generally used in contact-type applications such as welding and painting. The control block diagram of the impedance control is shown in Figure 5.

The controlled object in the admittance control is a position-controlled exoskeleton system. The exoskeleton system accepts force control information and outputs position information, which is characterized by mechanical impedance. The admittance controller and the impedance controller are dual, the input is the force information, and the output is the position information. According to formula (52), the transfer function of the admittance controller can be obtained:

$$\frac{\Delta\theta(s)}{T_{\text{int}}(s)} = \frac{1}{M(s)s^2 + B(s)s + K}. \tag{53}$$

Among them, $\Delta\theta$ represents the output of the

admittance controller, which is used to correct the reference trajectory θ_r to obtain the real desired trajectory θ_d of the position controller. The control block diagram of the admittance control is shown in Figure 6.

The most basic purpose of using the admittance controller is to achieve the effect of man-machine following, so the input force information of the admittance controller is the interaction force between man and machine. The interactive force information can be obtained by three-dimensional force sensors installed on the exoskeleton. The size of the trajectory correction output by the admittance model depends on the choice of admittance parameters and the magnitude of the interaction force between the human and the machine, which reflects the movement intention of the human body. Therefore, the compliant interaction between humans and machines can be achieved by selecting appropriate admittance parameters. It can be seen from Figure 6 that the admittance controller needs to be used in conjunction with the position tracker; that is, the position tracking control of the joint needs to be realized before the admittance control can be used. In addition, existing experience shows that the performance of the underlying positioner largely determines the performance and stability of the admittance control.

In order to study the influence of the admittance parameters M, B, and K on the control performance of the system, the simulation experiments are carried out for exploration. Since the exoskeleton is a human-machine integrated device, in order to fully describe the human-machine interaction performance of the entire system, the participation of the human body is required. However, the actual human dynamics modeling is very complicated. In order to not lose generality, a light spring is used to characterize the dynamic interaction performance of human muscles. The underlying position controller adopts the backstepping controller described in Section 2. In order to be closer to the actual situation, the reference trajectory θ_r is set within the constraints, and the exoskeleton dynamics model is selected. The effects of inertia, damping, and stiffness on the control performance of the system are studied by the control variable method. The control block diagram of the entire simulation is shown in Figure 7.

Taking the knee joint as an example, the influence of three admittance parameters on the human-computer interaction force is analyzed. The simulation results are shown in Figures 8–10. It can be seen from Figure 8 that the stiffness coefficient reflects the degree of adaptation of the exoskeleton to the environment. The greater the stiffness, the smaller the trajectory adjustment amount, but the longer the corresponding adjustment time. The stiffness coefficient reflects the "bounce" property of the exoskeleton. The greater the stiffness, the stronger the mechanical sense of the exoskeleton. The stiffness is small, and the flexibility of the exoskeleton is strong, indicating that the exoskeleton is easily dragged by the environment at this time. It can be seen from Figure 9 that the damping coefficient reflects the adaptation speed of the exoskeleton to the environment. The larger the damping coefficient, the longer the adjustment time and the more energy the system needs to consume. The damping coefficient reflects the characteristics of the "stickiness" of the exoskeleton. The larger the damping, the greater the damping force of the exoskeleton when the speed is fast. The smaller the damping, the smaller the damping effect when the exoskeleton is moving. It can be seen from Figure 10 that the inertia coefficient reflects the "heavy or not heavy" characteristics of the exoskeleton. The larger the inertia coefficient, the more torque needs to be continuously applied in the initial stage to change the state, and a longer adjustment time is required after the state changes. The smaller the inertia coefficient, the easier it is to change the state of the exoskeleton. However, according to formula (52), the change of the inertia coefficient will lead to a drastic change of the natural frequency and damping ratio, so it is not recommended to incorporate the inertia coefficient into the adjustable admittance parameters in the actual admittance control.

In the simplified schematic diagram of human-machine coupling shown in Figure 11, it can be seen that the human exoskeleton is bound together by flexible straps. Under passive control, the residual muscle strength of the affected limb and the driving force of the exoskeleton act together to drive the human body and the exoskeleton to move.

The motion intention of directly reacting with the human-computer interaction force is not reasonable enough, and the following modified admittance model can be considered, and (50) and (51) are revised and rewritten as follows:

$$\begin{cases} M\Delta\ddot{\theta}(t) + B\Delta\dot{\theta}(t) + K\Delta\theta(t) = \alpha T_{\text{int}}, \\ \Delta\theta(t) = \theta_d(t) - \theta_r(t). \end{cases} \tag{54}$$

Among them, θ_d represents the desired trajectory of the exoskeleton, that is, the input signal of the position controller, and α represents the coefficient of the human-computer interaction torque; that is, the modified interaction torque is used to represent the human intention. θ_r represents the reference trajectory, that is, the reference trajectory that can be dynamically designed by the medical staff according to the tennis-teaching situation.

In order to simplify the dynamic model of human muscles and simulate the actual interaction force in the simulation, as shown in Figure 10, without loss of generality, the dynamic interaction between the human body and the exoskeleton is expressed in the form of a spring damper.

$$T_{\text{int}} = K_{he}(\theta_h - \theta_e) + B_{he}\left(\dot{\theta}_h - \dot{\theta}_e\right). \tag{55}$$

Among them, $T_{\text{int}} = [T_{\text{hip}}; T_{\text{keen}}]$ represents the human-computer interaction torque, which can be measured by the three-dimensional force sensor in practice; $\theta_h \in R^{2\times 1}$ represents the human body angle; and $\theta_e \in R^{2\times 1}$ represents the angle information of the exoskeleton, which can be measured by the encoder in practice. $K_{he} \in R^{2\times 2}$ is the spring

stiffness coefficient, and $B_{he} \in R^{2\times2}$ is the damping coefficient.

4. Intelligent Teaching of Tennis Based on Human Skeleton Node Model

After processing the region-growing algorithm, the global foreground image of the tennis player is obtained. The athlete-centered background color removal is shown in Figure 12(a). In order to build the PSO-SVM tennis-training model, first, we need to extract the training set and test set from the obtained raw data. Then, we carry out a certain data analysis and preprocessing, use the training set to train the PSO-SVM network, and finally use the obtained model to test and analyze the test data. The flowchart is shown in Figure 12(b).

On the basis of the above research, an experiment is designed to test the model in this paper, and the tennis action correction effect and tennis-teaching effect of the tennis intelligent teaching model based on the human skeleton node model are, respectively, verified, and the results shown in Tables 1 and 2 are obtained.

From the above experimental research, it can be seen that the tennis intelligent teaching model based on the human skeleton node model has good effects in tennis action correction and tennis-teaching effect improvement.

5. Conclusion

The teaching goal of tennis option courses in colleges and universities is generally to let students learn and master certain basic theoretical knowledge of tennis and learn basic tennis-refereeing methods and game rules through tennis teaching. Moreover, it hopes that students can master basic physical exercise methods, improve health, and enhance physical fitness through the study of tennis techniques and tactics. At present, traditional teaching methods are mostly used in the teaching of tennis optional courses in colleges and universities; that is, through the explanation and demonstration of tennis technical movements by teachers, students follow the teaching process of teachers to perform collective imitation exercises. In this teaching process, teachers are the main body of teaching activities, and students are in a state of passively receiving knowledge. Under the background of talent training in the new era, the reform of tennis-teaching methods in colleges and universities is imminent. In this paper, the construction of a tennis intelligent teaching model is combined with the human skeleton node model. The experimental research results show that the tennis intelligent teaching model based on the human skeletal node model has good effects in tennis action correction and tennis-teaching effect improvement.

Data Availability

The labeled dataset used to support the findings of this study are available from the corresponding author upon request.

Conflicts of Interest

The authors declare no competing interests.

References

[1] O. Cant, S. Kovalchik, R. Cross, and M. Reid, "Validation of ball spin estimates in tennis from multi-camera tracking data," *Journal of Sports Sciences*, vol. 38, no. 3, pp. 296–303, 2020.

[2] E. E. Cust, A. J. Sweeting, K. Ball, and S. Robertson, "Machine and deep learning for sport-specific movement recognition: a systematic review of model development and performance," *Journal of Sports Sciences*, vol. 37, no. 5, pp. 568–600, 2019.

[3] N. Elliott, S. Choppin, S. Goodwill, T. Senior, J. Hart, and T. Allen, "Single view silhouette fitting techniques for estimating tennis racket position," *Sports Engineering*, vol. 21, no. 2, pp. 137–147, 2018.

[4] T. Fernando, S. Denman, S. Sridharan, and C. Fookes, "Memory augmented deep generative models for forecasting the next shot location in tennis," *IEEE Transactions on Knowledge and Data Engineering*, vol. 32, no. 9, pp. 1–1797, 2020.

[5] R. Gayanov, K. Mironov, R. Mukhametshin, A. Vokhmintsev, and D. Kurennov, "Transportation of small objects by robotic throwing and catching: applying genetic programming for trajectory estimation," *IFAC-Papers OnLine*, vol. 51, no. 30, pp. 533–537, 2018.

[6] B. Giles, S. Kovalchik, and M. Reid, "A machine learning approach for automatic detection and classification of changes of direction from player tracking data in professional tennis," *Journal of Sports Sciences*, vol. 38, no. 1, pp. 106–113, 2020.

[7] Y. F. Ji, J. W. Zhang, Z. Shi, M. H. Liu, and J. Ren, "Research on real–time tracking of table tennis ball based on machine learning with low-speed camera," *Systems Science & Control Engineering*, vol. 6, no. 1, pp. 71–79, 2018.

[8] M. R. Keyvanpour, S. Vahidian, and M. Ramezani, "HMR-vid: a comparative analytical survey on human motion recognition in video data," *Multimedia Tools and Applications*, vol. 79, no. 43-44, pp. 31819–31863, 2020.

[9] S. A. Kovalchik, J. Sackmann, and M. Reid, "Player, official or machine?: Uses of the challenge system in professional tennis," *International Journal of Performance Analysis in Sport*, vol. 17, no. 6, pp. 961–969, 2017.

[10] J. P. R. Lara, C. L. R. Vieira, M. S. Misuta, F. A. Moura, and R. M. L. . Barros, "Validation of a video-based system for automatic tracking of tennis players," *International Journal of Performance Analysis in Sport*, vol. 18, no. 1, pp. 137–150, 2018.

[11] M. F. López, "Research on the specific movement of the head in tennis strokes," *ITF Coaching & Sport Science Review*, vol. 28, no. 80, pp. 16–19, 2020.

[12] M. R. Mohammadi, "Deep multiple instance learning for airplane detection in high-resolution imagery," *Machine Vision and Applications*, vol. 32, no. 1, pp. 1–14, 2021.

[13] G. Tsagkatakis, M. Jaber, and P. Tsakalides, "Convolutional neural networks for the analysis of broadcasted tennis games," *Imaging*, vol. 30, no. 2, pp. 206-1–206-6, 2018.

[14] R. L. Yan, "An artificial intelligence and machine vision based evaluation of physical education teaching," *Journal*

of Intelligent & Fuzzy Systems, vol. 40, no. 2, pp. 3559–3569, 2021.

[15] J. Zhang, H. Yu, H. Deng, Z. Chai, M. Ma, and X. Zhong, "A robust and rapid camera calibration method by one captured image," *IEEE Transactions on Instrumentation and Measurement*, vol. 68, no. 10, pp. 4112–4121, 2019.

[16] Y. Zhao, R. Xiong, and Y. Zhang, "Model based motion state estimation and trajectory prediction of spinning ball for ping-pong robots using expectation-maximization algorithm," *Journal of Intelligent & Robotic Systems*, vol. 87, no. 3-4, pp. 407–423, 2017.